J Theor Appl Phys (2016) 10:129–137
DOI 10.1007/s40094-016-0210-3

RESEARCH

Calculating formation range of binary amorphous alloys fabricated by electroless plating

Bangwei Zhang[1] · Shuzhi Liao[2] · Xiaolin Shu[3] · Haowen Xie[2]

Received: 6 April 2015 / Accepted: 23 January 2016 / Published online: 16 February 2016

Abstract A lot of amorphous alloy deposits in the binary (Ni, Co, Cu)–(P, B) alloy systems fabricated by electroless plating (EP) have been reported up to date. But no one reported their theoretical modeling of the amorphous formation and calculated their concentration range of amorphous formation (RAF). Using Miedema model and subregular model scheme, the RAFs for the six EP (Ni, Co, Cu)–(P, B) alloys and three Ni–Cu, Ni–Co and Co–Cu alloys have been calculated systematically for the first time. The calculated results are in agreement with experimental observations. Experiments and calculations for the RAFs in the latter three alloy systems reveal that not any RAF formed except crystalline states. The huge difference between the six metal–metalloid alloys and three metal–metal alloys in RAF has been discussed in detail in the paper.

Keywords Binary amorphous alloys · Electroless plating · Miedema model and subregular model scheme · Range of amorphous formation

✉ Bangwei Zhang
zbw1212@126.com

[1] College of Physics, Hunan University, Changsha 410082, People's Republic of China

[2] Key Laboratory of Quantum Structures and Quantum Control of Ministry of Education, Department of Physics, Hunan Normal University, Changsha 410081, People's Republic of China

[3] Department of Physics, Beijing University of Aeronautics and Astronautics, Beijing 100083, People's Republic of China

Introduction

Just after discovering the electroless plating (EP) Ni–P alloy deposits by Brenner and Riddell [1], Gutzeit and Mapp [2] measured the composition and structure of 'Kanigen' coating by X-ray and electron diffraction. They found that Kanigen coatings have the structure of an amorphous, solid substance with liquid-like disorder of the atoms. Up to date, a lot of EP amorphous alloy deposits and their concentration ranges including binary, ternary and quaternary alloy coatings have been reported. Table 1 lists the experimental data of the range of amorphous formation (RAF) for the most important nine EP binary Ni–P, Ni–B, Co–P, Co–B, Cu–P, Cu–B, Ni–Cu, Ni–Co and Co–Cu alloy systems, which will be analyzed and theoretically modeled in this paper. Several features can be found from this measured data list, but they will be illustrated in the below text.

It is well known that comparing to its crystalline phase counterpart an amorphous alloy prepared by any one method can have specific superior properties. Therefore, if the RAF in an alloy system is large, then every alloy in the RAF must be in the amorphous state, and the properties of the alloy system definitely have advantages. That is to say, it is also very important to study the RAF in the EP. This may be because people paid much attention to measure the RAF in EP. The data in Table 1 just illustrate some of them which will be considered in the paper.

The problem is that nearly 70 years after discovering the EP Ni–P alloy deposits by Brenner and Riddell, almost no one reported the theoretical model and calculations of the RAF in EP alloy deposits up to date. This situation is somewhat strange because people have been measuring a lot of the RAF in EP alloy coatings. In addition, as described in the above paragraph, either from the

Table 1 Composition, structure and formation range of amorphous phases for nine EP alloy deposits [3–21]

No.	Experimental data										Calculated results	
	Alloys	Parameters		Data					RAF, at.%	Refs.	RAF, at.%	Refs.
1	Ni–P	Composition	P, at.%	30.8	26.5	15.8	14.2	10.8	26.5–30.8 P	[3]	18–88	Present
		Structure		A	A	C	C	C				
2	Ni–P	Composition	P, at.%	20.8	13.3	6.4			20.8 P	[4]		
		Structure		A	A + C	C						
3	Ni–P	Composition	P, at.%	22.5	12		6.2		22.5 P	[5]		
		Structure		A	Micro C		C					
4	Ni–P	Composition	P, at.%	12	20				20 P	[6]		
		Structure		C	A matrix							
5	Ni–P	Composition	P, at.%	4.0	6.9	13.8			13.8 P	[7]		
		Structure		C	C	A						
6	Ni–P	Composition	P, at.%	21.5	18.4	12.3				[8]		
		Structure	C, nm	5.2	7.8	17						
7	Ni–P	Composition	P, at.%	8.03	12.53	23.09	27.42	28.71	12.53–28.71 P	[9]		
		Structure		C	A	A	A	A				
8	Ni–B	Composition	B, at. %	19.6	24.7	27.1			24.7–27.1 B	[10]	10–90	Present
		Structure		C	A	A						
9	Ni–B	Composition	B, at.%	31	41	42			41 B	[11]		
		Structure		C	A	A						
10	Ni–B	Composition	B, at.%	5.5	7.9	12.9		17.1	17.1 B	[12]		
		Structure		C	Micro C	Micro C		A				
11	Ni–B	Composition	B, at.%	2.26	21	25			25 B	[13]		
		Structure		C	C	A						
12	Ni–B	Composition	B, at.%	14.4	24.1		26.6		26.6 B	[14]		
		Structure		C	Micro C + A		A					
13	Co–P	Composition	P, at.%	~10	10–12		>12		about 12 P	[15]	20–90	Present
		Structure		C	Part A		Total A					
14	Co–P	Composition	P, at.%	14.6	15.1	15.9	16.5	17.1	16.5–17.1 P	[16]		
		Structure		C	C	C	A	A				
15	Co–B	Composition	B, at.%	2.26	22	25.8			25.8 B	[13]	24–68	Present
		Structure		C	C	A						
16	Co–B	Composition	B, at.%	5.1					5.1 B	[17]		
		Structure		A								
17	Cu–P	Composition	P, wt.%	1.55 (Cu 79.11, others are: Fe, O and C in the coating)						[18]	20–86	Present
		Structure		C								
18	Cu–B	Composition	B, at.%	No one measured the amorphous formation and RAF in the EP Cu–B system							10–91	Present
		Structure										
19	Cu–Ni	Composition	Ni, wt.%	28–37.8						[19]	No RAF	Present
		Structure		C								
20	Ni–Co	Composition	Ni, at.%	0–100						[20]	No RAF	Present
		Structure		C (fcc or hcp)								
21	Ni–Co	Composition	Ni, at.%	~40–60						[21]		
		Structure		C								
22	Co–Cu	Composition	Cu, at.%	No one measured the amorphous formation and RAF in the EP Co–Cu system							No RAF	Present
		Structure										

C crystalline state, *A* amorphous state

theoretical view point or from the practice application, the description and calculation for the formation range of EP amorphous alloys are very important. So, one may say with a little pity that there is a theoretical gap for the theoretical calculation of formation range of such amorphous alloy systems.

The reason for this problem is somewhat strange as said above, it is because the situation is different with that in the conventional amorphous alloys prepared by melt quenching (MQ) and mechanical alloying (MA) methods. Perhaps the number of the manufactured conventional amorphous alloy systems is more in quantity, but the studies of the RAF in such alloy systems are also not few. For example, Johnson's group in 2003 [22] used the magnitude of atomic size ratio of $0.60 < \lambda < 0.95$ to predict the RAF of Cu binary and ternary alloys from the melt. Kim et al. [23] proposed a new thermodynamic calculation scheme to estimate the composition dependency of glass forming ability in multicomponent alloy systems. Rao et al. [24] predicted the best glass forming composition identified by drawing iso-Gibbs energy change contours by representing quinary systems as pseudo-ternary ones. Sun et al. [25] calculated the RAF in Al–Ni–RE (Ce, La, Y) ternary alloys and their sub-binaries based on Miedema's model. Das et al. [26] also used the Miedema model-based methodology to predict amorphous-forming composition range in ternary systems of MA Al–Ni–Ti alloys.

It is obvious that a great deal of attention has been drawn to investigate the RAF of amorphous alloy systems manufactured by MQ and/or MA techniques. However, nearly no one reported the theoretical model and calculations of the RAF in EP alloy deposits up to date.

That is why we calculate systematically the RAF of EP alloy systems listed in Table 1 for the first time, and discuss the obtained results in detail in the paper.

Theoretical model

Using the scheme to calculate the RAF with the Miedema model for the heat of mixing of binary alloys proposed by Miedema and co-workers [27], our group in 2002 [9] calculated the RAF of EP Ni–P alloy deposits. The key of the scheme for estimating the RAF is to compare the free energies of the crystalline and amorphous phases. Because the entropy contribution to the free energy is very small at the room temperature of 300 K the driving force for amorphization comes mainly from the enthalpy contribution. We, therefore, just calculated the enthalpy-composition plots instead of the free energy-composition plots in this study. The enthalpies of solid solution can be represented as [28]

$$\Delta H_{AB} = \Delta H^{c}_{AB} + \Delta H^{e}_{AB} + \Delta H^{s}_{AB} \tag{1}$$

where the superscripts c, e and s correspond to the chemical, elastic and structure contributions to the enthalpy of solid solution, respectively. It is obvious that crystalline pure elements were chosen to be the standard state and their enthalpies were assigned to be zero in the calculations, hence providing the representation of Eq. (1). The equation of the chemical interaction contribution to the enthalpy of a solid solution derived and used by Miedema belongs to the regular model (Eq. (2.25) in [29]). However, we used the subregular model for calculating the mixing enthalpies [30]:

$$\Delta H^{c}_{AB} = x_A x_B (x_A \Delta H^{0}_{B\text{in}A} + x_B \Delta H^{0}_{A\text{in}B}) \tag{2}$$

where x_A and x_B are the contents of compositions A and B, respectively. $\Delta H^{0}_{A\text{in}B}$ is the enthalpy of solution of one element A in other element B at an infinite dilution for a binary alloy system, which can be calculated from the Miedema model [29]. Correspondingly $\Delta H^{0}_{B\text{in}A}$ is for element B in element A.

The elastic contribution to the enthalpy arises from the difference in atomic volume between the solute and the solvent. Similarly, it can be presented as

$$\Delta H^{e}_{AB} = x_A x_B (x_A \Delta H^{e}_{B\text{in}A} + x_B \Delta H^{e}_{A\text{in}B}) \tag{3}$$

where $\Delta H^{e}_{A\text{in}B}$ is the size-mismatch contribution to the enthalpy of solution in a binary system. The Friedel formalism [31] is given by

$$\Delta H^{e}_{AB} = \frac{24\pi B_A \mu_B R_A R_B (R_A - R_B)^2}{3B_A R_B + 4\mu_B R_A} \tag{4}$$

where B_A is the bulk modulus of the solute, and μ_B the shear modulus of the solvent, for which their values have been tabulated by Gschneidner [32]. R_A and R_B are the radii of the solute and solvent, respectively.

ΔH^{s}_{AB} in Eq. (1) is a structural contribution to the enthalpy of the alloys taking into account the difference between the valences and the crystal structure of the solute and solvent. The latter is expected to have only a minor effect when compared with the elastic energy contribution [33]. Further, it is difficult to calculate the structure contribution. Therefore, this term will not be considered in the calculation, as a first approximation.

As for the enthalpy of amorphous alloy, there are no contributions from the elastic and structural terms, so that its enthalpy of formation can be written as

$$\Delta H^{a}_{AB} = \Delta H^{a,c}_{AB} + \Delta H^{a}_{A} + \Delta H^{a}_{B} \tag{5}$$

where ΔH^{i}_{A} is the enthalpy of the amorphous pure element i. According to van der Kolk et al. [34], it is given by

$$\Delta H_A^i = \alpha T_{m,i} \tag{6}$$

where $\alpha = 3.5$/mol K, and $T_{m,i}$ is the melting temperature of element i. $\Delta H_{AB}^{a,c}$ is the chemical contribution to the enthalpy of the amorphous alloy. Considering the short-range order observed in the amorphous phases [35], it is given by

$$\Delta H_{AB}^{a,c} = \Delta H_{AB}^{c}[1 + 5(x_A^s x_B^s)^2] \tag{7}$$

where

$$x_A^s = \frac{x_A V_A^{2/3}}{x_A V_A^{2/3} + x_B V_B^{2/3}} \tag{8}$$

$$x_B^s = 1 - x_A^s \tag{9}$$

in which x_i^s is the surface concentration of element i, where V_i is the volume of the element i.

Calculated results and discussions

Before describing the theoretical results of RAF in binary EP alloys, a problem left in "Theoretical model'', i.e., the features from the measured data will be discussed first. One of the features is that many groups measured the RAF for one alloy system, e.g., seven groups measured the RAF in EP Ni–P alloys. However, only one paper for the EP Cu–P and Ni–Cu alloys has been published to date. In addition, no other reporters of RAF can be found for the EP Cu–B and Co–Cu alloy systems.

The second feature is that the data of the RAF of binary EP amorphous alloys measured from various author groups are not the same, but usually are different. For example, the lower limitation of P for Ni–P in Nos. 5 and 7 in Table 1 is 13–14 at.%, but that in No. l is 26.5 at.%; those of B for Ni–B in Nos. 10 and 9 are 17.1 and 41 at.%, and those of B for Co-B in Nos. 16 and 15 are 5.1 and 25.8 at.%, respectively. The reasons are that the preparation techniques of samples are difficult, not the same; moreover, the measurement error is difficult to avoid from different authors.

The third feature is that there is only the lower limitation, but no upper limitation for the RAF of EP binary amorphous alloys. Most of the measured data for the RAF of EP binary amorphous alloys are containing one TM (Ni, Co or Cu) and one metalloid (P or B). P and B are the easy formation amorphous elements, and the more the content of P or B in the deposits, the easier to form amorphous phase. Once the deposits became full amorphous state, adding more content of P or B in the deposits cannot turn them into crystal but still maintains their amorphous phase. Therefore, no upper limitation of metalloid in such binary amorphous deposits can be reached. In fact, the EP binary amorphous deposits, e.g., Ni–P with very high content of P (>80 at.%) have not been reported to date because of the experimental difficulty.

The last feature is that though many experimental data for the RAF of binary EP amorphous alloys have been reported as shown in Table 1, the explanations to the experimental data nearly cannot be found in the literature. That is why we present this study.

The enthalpy-composition diagrams have been calculated for all nine binary Ni–P, Ni–B, Co–P, Co–B, Cu–P, Cu–B, Ni–Cu, Ni–Co and Co–Cu alloy systems to predict the range of amorphous formation, as shown in Figs. 1, 2, 3 and 4. The RAF of every EP alloy system is summarized in Table 1 too.

Theoretical calculations show that the RAF of the six binary EP (Ni, Co, Cu)–(P, B) alloys is 18–88, 10–90, 20–90, 24–68, 20–86 and 10–91 at.% P or B, respectively. The experimental data are all included in the calculated RAF. It can be seen that the predicted lower limitation of RAF from the theoretical calculation is P 18 at.%, which is generally in agreement with the most of the measured results. But others are not so in agreement with the experimental results. This is easy to understand. Firstly, it is well known that the enthalpies calculated from the Miedema model cause some errors, as Miedema himself accepted [29]. This part of the error comes from the electronic reactions between atoms, usually the error range between the calculated and experimental values of enthalpies is about 10–20 % [36, 37], so it is the important part in the errors. On the other hand, the elastic term of enthalpy is calculated using the Friedel formalism obtained from the theory of elasticity. It is expected that this term will cause some errors in the calculations of enthalpy. However, it estimated a rather small impact to the enthalpy corresponding to that from the Miedema model [36]. Furthermore, the neglect of the structure term in the enthalpy and the effect of temperature on the enthalpy would also produce some errors on the calculations, for which the effect to the enthalpy is also rather small. All of these will make the calculated enthalpies somewhat different from the practical values for the alloys. In addition, considering the dispersion of experimental data by various groups as shown in Table 1, we can say that the theoretically predicted RAF is pretty good in agreement with the experimental results.

Theoretical calculation also indicates that the upper limitation of RAF for these six binary EP (Ni, Co, Cu)–(P, B) alloys is very high, around 90 at.% of metalloid elements. In addition, the measured upper limitation of RAF is less than that from the calculated results. The three reasons have been mentioned in the discussion.

No one has measured the amorphous formation and RAF in the EP Cu–B system until now, so no experimental

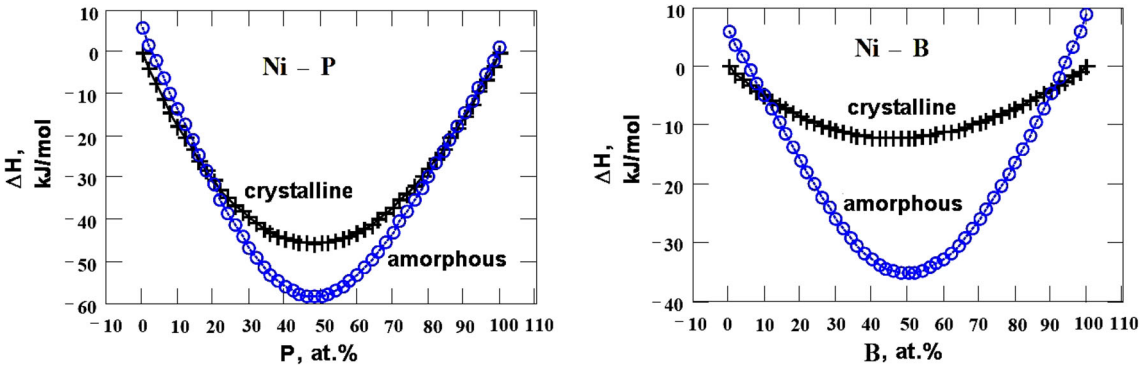

Fig. 1 Formation range of amorphous alloys Ni–P and Ni–B prepared by electroless plating

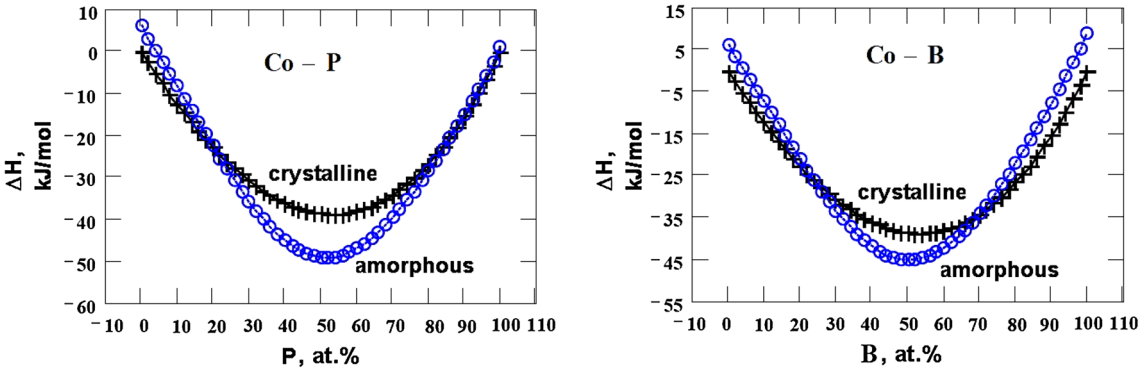

Fig. 2 Formation range of amorphous alloys Co–P and Co–B prepared by electroless plating

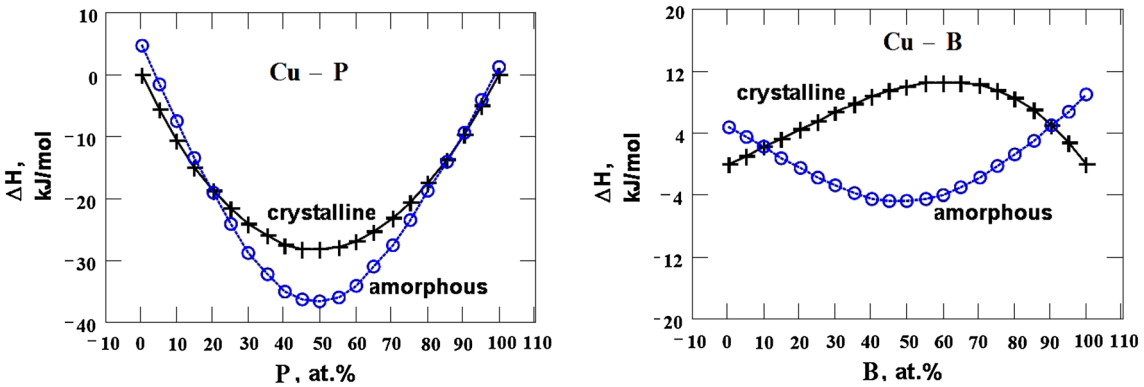

Fig. 3 Formation range of amorphous alloys Cu–P and Cu–B prepared by electroless plating

data can be compared with the calculated results. Soheila et al. [18] in 2011 reported the EP Cu–P alloys, and they only obtained a crystalline Cu–P coating with 1.55 wt.% P (Cu 79.11 wt.%, others are: Fe, O and C in the coating). It is obvious that this crystalline alloy locates outside the calculated RAF of EP Cu–P. This author in 2014 [38] published another similar paper on EP Cu–P coating, still no other compositions in the coating can be found in that paper. Either EP Cu–P or Cu–B alloy coatings are needed to further measure the RAFs to further confirm that if the present calculations are really effective in these two EP alloy systems.

As for the Ni–Cu, Ni–Co and Co–Cu alloy systems, the calculations show that no amorphous alloys can be formed because all the ΔH curves of amorphous phases are wholly above those of crystalline states. In these three systems, Ni–Cu and Ni–Co alloy systems have been studied by EP [19–21]. Nawafune et al. found that the structure of EP Ni–

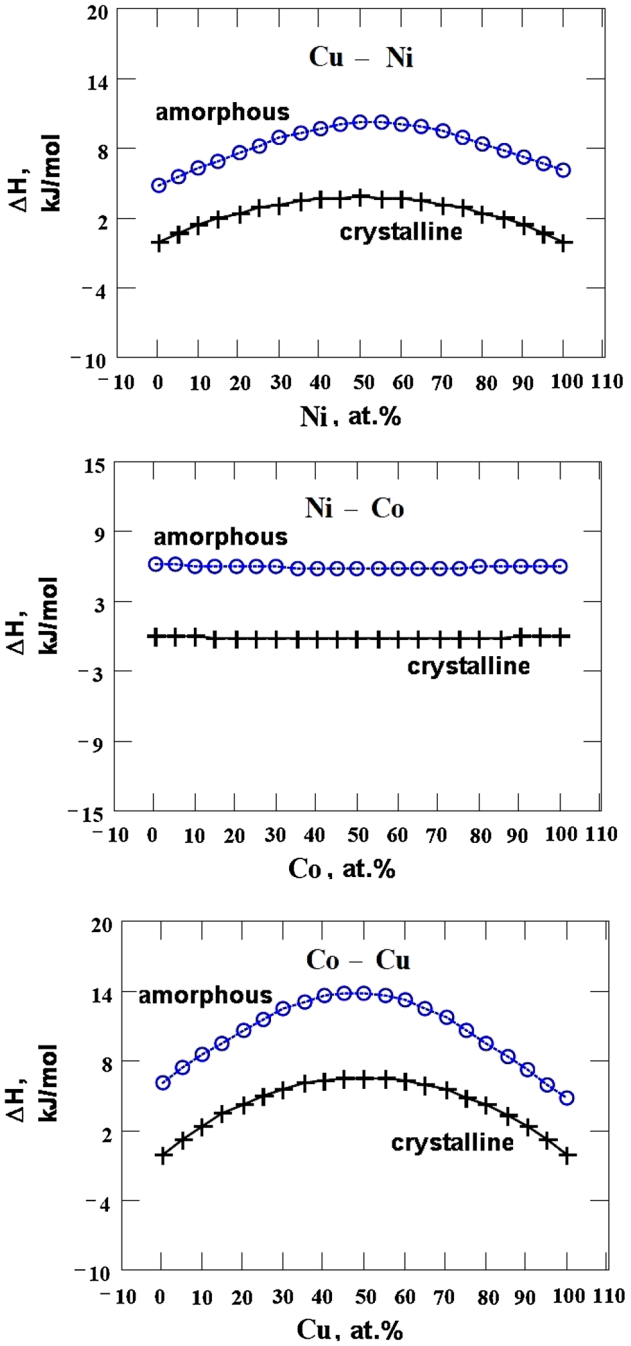

Fig. 4 Formation range of amorphous alloys Cu–Ni, Ni–Co and Co–Cu prepared by electroless plating

Cu coatings is crystalline for the compositions of Ni in 28–37.8 wt.%, which is in agreement with the calculated results. Yagi et al. [20] and Kim et al. [21] studied the EP Ni–Co systems, respectively. The composition of the EP coatings ranges from ~40 to 60 at.% Ni by Yagi et al., and all of the coatings in the range are crystalline phases. Kim et al. prepared the EP Ni–Co coatings covering the whole composition range from 0 to 100 at.% Ni, with all crystalline state structures (fcc or hcp). It is obvious that the calculations are completely in agreement with the measured data.

Of these three alloy systems, only for the Co–Cu system no paper on its EP investigation has been found to date. But, there are few studies on the system using electrodeposition. The experimental data show no RAF but only crystalline phases can be obtained. For example, Gómez et al. [39] prepared Co–Cu alloy thin films using electrodeposition method. Their results indicated that the composition of 12–30 wt.% Co in the coatings, and a solid solution in a fcc-like structure is formed in the electrodeposition conditions, although TEM analysis showed the random distribution of nanometric dense particles of cobalt distributed within the deposits. Almasi Kashia et al. [40] also investigated the Cu content of electrodeposited Co–Cu alloy nanowire arrays fabricated by ac pulse electrodeposition. The Co content of the nanowire arrays is in a wide range from 7 to 53 wt.%. They also found that the fabricated Co–Cu nanowires with mixed phase of hcp Co, fcc Cu and fcc Co–Cu crystal phase. From the Co–Cu equilibrium phase diagram [41], it can be seen that Co and Cu present immiscibility and do not form any intermetallic compound, which revealed that there is a very limited interaction between the constituents Co and Cu of the metallic alloy Co–Cu coatings. Why the interaction between the constituents Co and Cu in the Co–Cu alloy is not strong? Firstly, the electron factors of these two constituents Co and Cu are not very different but rather similar. Secondly, the radius of Co and Cu are 0.125 and 0.128 nm, making their size factors nearly equal. Thirdly, although Co and Cu have different crystal structures (hcp vs. fcc), such difference is expected to have only a minor effect when compared with the size factor contribution [33]. All of these reasons make the interaction between Co and Cu rather weaker, and make their atoms difficult to attract each other together and form a tight group of atoms during electrodeposition process, thereby no amorphous states can be formed. Of course, such weaker attraction between Co and Cu cannot result in an intermetallic phase in Co–Cu alloy system because it is usually considered that more strong attraction results in an intermetallic phase. As for the first- and second-mentioned points we will analyze them more in detail below.

To understand the calculation results and comparing them with the experimental data more clearly, the plot of these nine EP binary amorphous formation [42] is given in Fig. 5. When one of the author (ZBW) investigated the theory of formation for amorphous alloy systems produced by melt quenching (MQ), ion beam mixing (IBM) and other methods [43–45], he used a two-dimensional plot scheme. The two chemical coordinates are $X = |(R_A - R_B)/R_A|$ and $Y = |10|\Delta\Phi| - 30|\Delta n^{-1/3}||$, where R

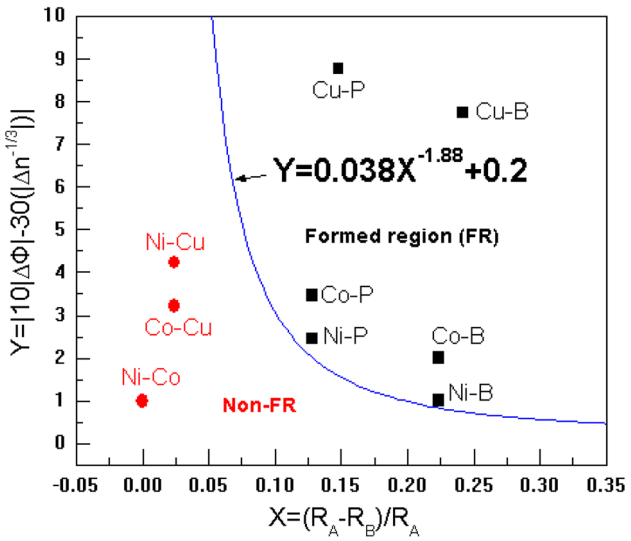

Fig. 5 Amorphous formation plot of binary EP alloys by chemical coordinates

is the atomic radium, $n^{-1/3}$ and Φ are the two Miedema coordinates. Y and X are the electron and size factors, respectively. These two factors are just used to represent the interaction between two constituents in a binary alloy. The electron factor is determined by the bond effect, the difference in electronegativity and the alloying effect of an element. It represents the rather complex effects of the atomic nuclei on the outer and valence electrons, as well as the complex interactions between outer and valence electrons and between the ions themselves. They are generally connected with the behavior of electrons; therefore, ZBW calls them electron factor. It is obvious that if the difference between the electron factors of two kinds of atoms is large, the short-range interaction between the two dissimilar atoms then combines closely, and there is not enough motive force and enough time for the atoms in the group to move any great distance, or to rearrange cooperatively to produce a regular atomic configuration suitable for forming crystalline structure in longer distance. This means that crystallization is hindered thereby leading to easy formation of amorphous alloys. The size factor X indicates the difference of atomic size between two kinds of atoms. If X is large, the difference between the two atomic sizes is large, and the two dissimilar atoms combined more tightly together and the atomic group is more stable. It is, therefore, more difficult for the atoms in the group to move any large distance or to rearrange cooperatively. The formation of crystalline structure in longer distance is, therefore, impeded thereby leading to easy formation of amorphous alloys. That is why besides Y, the size factor has been also proved to play some role and must be considered in the formation of amorphous alloys. Considering together these two kinds of factors, i.e., Y and X, when they are large, the short-range interaction for the two dissimilar atoms is strong, the group of the dissimilar atoms then combine tightly. Therefore, it is more difficult for the atoms in the group to move any great distance, or to rearrange cooperatively to produce a regular atomic configuration suitable for forming crystalline structure in longer distance. That is to say, the formation of crystalline structure is hindered thereby leading to easy formation of amorphous alloys. From Fig. 5, six alloy systems (Ni–P, Ni–B, Co–P, Co–B, Cu–P and Cu–B) are all located in the amorphous formation region because their Y and X values are all rather large. However, the other three systems Ni–Cu, Ni–Co and Co–Cu are all located in the non-amorphous formed area as their Y and X values are all rather small. In such a question, the amorphous formation plot for the nine binary alloy systems further and more clearly explain the above calculation results on the RAF.

Conclusions

Using the Miedema model and subregular atom model scheme, the RAF of EP binary amorphous alloy systems has been modeled and calculated theoretically for the first time.

The calculated results show that six alloy systems Ni–P, Ni–B, Co–P, Co–B, Cu–P and Cu–B all have an RAF, which are in agreement with the experimental data except that there is no experimentally measured data in EP Cu–B system. In addition, the calculated RAFs are usually greater than those measured RAFs.

For the three metal–metal (Ni–Cu, Ni–Co and Co–Cu) alloys, measurements and calculations all show that not any amorphous phase can be formed except the crystalline states. The internal reactions between the atoms in these alloy systems decide such results.

It can be said from the results that the theoretical gap for the theoretical calculation of formation range of EP amorphous alloy systems has been filled to a certain content.

References

1. Brenner, A., Riddell, G.E.: Nickel plating on steel by chemical reduction. J. Res. Nat. Bur. Stand. **37**, 31 (1946)

2. Gutzeit, G., Mapp, E.T.: Chemical nickel plating. Anti-Corros. Methods Mater. **3**(10), 331 (1956)
3. Mimani, T., Mayanna, S.M.: The effect of microstructure on the corrosion behaviour of electroless Ni–P alloys in acidic media. Surf. Coat. Technol. **79**, 246 (1996)
4. Gao, Y., Zheng, Z.J., Zhu, M., Luo, C.P.: Corrosion resistance of electrolessly deposited Ni–P and Ni–W–P alloys with various structures. Mater. Sci. Eng. A **381**, 98 (2004)
5. Antonelli, S.B., Allen, T.L., Johnson, D.C., Johnson; Dubin, V.M.: Determining the role of W in suppressing crystallization of electroless Ni–W–P films. J. Electrochem. Soc. **153**(6), J46 (2006)
6. Sankara Narayanana, T.S.N., Baskaran, I., Krishnavenia, K., Parthiban, S.: Deposition of electroless Ni–P graded coatings and evaluation of their corrosion resistance. Surf. Coat. Technol. **200**, 3438 (2006)
7. Fundo,.A.M., Abrantes, L.M.: The electrocatalytic behaviour of electroless Ni–P alloys. J. Electroanal. Chem. **600**, 63 (2007)
8. Cheng, Y.H., Zou, Y., Cheng, L., Liu, W.: Effect of the microstructure on the properties of Ni–P deposits on heat transfer surface. Surf. Coat. Technol. **203**(12), 1559 (2009)
9. Haowen, X., Bangwei, Z.: Effects of preparation technology on the structure and amorphous forming region for electroless Ni–P alloys. J. Mater. Proc. Technol. **124**, 8 (2002)
10. Gorbunova, K.M., Ivanov, M.V., Moiseev, V.P.: Electroless deposition of Nickel–Boron alloys. J. Electrochem. Soc. **120**(5), 613–618 (1973)
11. Watanabe, T., Tanabe, Y.: Formation and morphology of Ni–B amorphous alloy deposited by electroless plating. Mater. Sci. Eng. **23**, 97 (1976)
12. Watanabe, T., Tanabe, Y.: The lattice images of amorphous-like Ni–B alloy films prepared by electroless plating method. Trans. Jpn. Inst. Metals **24**(6), 396 (1983)
13. Saito, T., Sato, E., Matsuoka, M., Iwakura, C.: Electroless deposition of Ni–B, Co–B and Ni–Co–B alloys using dimethylamineborane as a reducing agent. J. Appl. Electrochem. **28**(5), 559 (1998)
14. Wang, Z.C., Jia, F., Yu, L., Qi, Z.B., Tang, Y., Song, G.-L.: Direct electroless nickel–boron plating on AZ91D magnesium alloy. Surf. Coat. Technol. **206**, 3676 (2012)
15. Chekanova, L.A., Denisova, E.A.: Magnetic properties of electroless fine Co–P particles. IEEE Trans. Mag. **33**(5), 3730 (1997)
16. Peng, Z., Zeng Guo, Z., Defang, W., Nacan, H., Shenjun, H., Guitong, W.: Amorphous conditions and performance of electroless Co–P alloy deposit. Mater. Prot. **32**(12), 4 (1999)
17. Tianpeng, X., Lei, Z., Qiuhua, H.: Effect of rare earth metals on structure and properties of electroless Co–B alloy coating. J. Rare Earths **20**(5), 512 (2002)
18. Soheila, F., Rahim, A.A., Mohamed, N., Sipaut, C.S., Raja, B.: The influence of SiC particles on the corrosion resistance of electroless, Cu–P composite coating in 1 M HCl. Mater. Chem. Phys. **129**, 1063 (2011)
19. Hidemi, N., Takashi, U., Shozo, M., Masami, I., Tsuneshi, N.: Electroless copper–nickel binary alloy plating and electrical resistance properties. Jpn. J. Surf. Finish. **49**(7), 796 (1998)
20. Yagi, S., Kawamori, M., Matsubara, E.: Electrochemical study on the synthesis process of Co–Ni alloy nanoparticles via electroless deposition. J. Electrochem. Soc. **157**(5), E92 (2010)
21. Dong-uk, K., Rajakumar, S., Myung-Ryul, C., Bongyoung, Y.: Formation of Co–Ni alloy thin films on silicon by electroless deposition. Electrochim. Acta **75**, 42 (2012)
22. Hyon-Jee, L., Cagin, T., Johnson, W.L., Goddard III, W.A.: Criteria for formation of metallic glasses: the role of atomic size ratio. J. Chem. Phys. **119**(18), 9858 (2003)
23. Deok, K., Byeong-Joo, L., Nack, J.K.: Thermodynamic approach for predicting the glass forming ability of amorphous alloys. Intermetallics **12**, 1103 (2004)
24. Rao, B.S., Bhatt, J., Murty, B.S.: Identification of compositions with highest glass forming ability in multicomponent systems by thermodynamic and topological approaches. Mater. Sci. Eng. A **211**, 449–451 (2007)
25. Sun, S.P., Yi, D.Q., Liu, H.Q., Zang, B., Jiang, Y.: Calculation of glass forming ranges in Al–Ni–RE (Ce, La, Y) ternary alloys and their sub-binaries based on Miedema's model. J. Alloys Comp. **506**, 377 (2010)
26. Das, N., Mittra, J., Murty, B.S., Pabi, S.K., Kulkarni, U.D., Dey, G.K.: Miedema model based methodology to predict amorphous-forming-composition range in binary and ternary systems. J. Alloys Comp. **550**, 483 (2013)
27. Loeff, P.I., Weeber, A.W., Miedema, A.R.: Diagram of formation enthalpies of amorphous alloys in comparison with the crystalline solid solution. J. Less-Common. Met. **140**, 299 (1988)
28. Niessen, A.K., Miedema, A.R.: The enthalpy effect on forming diluted solid solution of two 4d and 5d transition metals. Ber. Bunsenges. Phys. Chem. **87**, 717 (1983)
29. de Boer, F.R., Boom, R., Mattens, W.C.M., Miedema, A.R., Niessen, A.R.: Cohesion in Metals, Transition Metal A1loys. North-Ho1land, Amsterdam (1988)
30. Zhang, B., Liao, S., Xie, H., Yuan, X., Shu, X.: A subregular model for calculating the mixing enthalpies in 10 binary IIB–IIIB alloy systems. EPL **89**, 56002 (2010)
31. Friedel, J.: Electronic structure of primary solid solutions in metals. Adv. Phys. **3**, 446 (1954)
32. Gschneidner Jr, K.A.: Physical properties and interrelationships of metallic and semimetallic elements. Solid State Phys. **16**, 275 (1964)
33. Murty, B.S., Ranganathan, S.R., Rao, M.M.: Solid state amorphization in binary Ti–Ni, Ti–Cu and ternary Ti–Ni–Cu system by mechanical alloying. Mater. Sci. Eng. A **149**, 231 (1992)
34. Van der Kolk, G.J., Miedema, A.R., Niessen, A.K.: On the composition range of amorphous binary transition metal alloys. J. Less-Common. Met. **145**, 1 (1988)
35. Weeber, A.W.: Application of the Miedema model to formation enthalpies and crystallisation temperatures of amorphous alloys. J. Phys. F **17**, 809 (1987)
36. Niessen, A.K., de Boer, F.R., Boom, R., de Chatel, P.F., Mattens, W.C.M., Miedema, A.R.: Model prediction for the enthalpy of formation of transition metal alloys II. CALPHAD **7**(1), 51 (1983)
37. Zhang, B.: Miedema theory for formation heat of alloy system. Shanghai Met. **15**(5), 23 (1993)
38. Soheila, F., Amir, H.F., Seyed, R.N.: An investigation on electroless Cu–P composite coatings with micro and nano-SiC particles. Mater. Des. **54**, 570 (2014)
39. Gómez, E., Labarta, A., Llorente, A., Vallés, E.: Electrodeposited cobalt + copper thin films on ITO substrata. J. Electroanal. Chem. **517**, 63 (2001)
40. Almasi Kashia, M., Ramazani, A., Adelnia Najafabadi, F., Heydari, Z.: Controlled Cu content of electrodeposited Co–Cu nanowires through pulse features and investigations of microstructures and magnetic properties. Appl. Surf. Sci. **257**, 9347 (2011)
41. Baker, H. (ed.): Alloy Phase Diagrams, ASM Handbook, vol. 3. ASM International, Ohio (1992)
42. Zhang, B.: Description of the formation of binary amorphous alloys by chemical coordinates. Physica **132B**, 319 (1985)
43. Zhang, B.: Application of Miedema's coordinates to the formation of binary amorphous alloys. Physica **121B**, 405 (1983)

44. Zhang, B.: A semi-empirical approach to the prediction of the amorphous alloys formed by ion beam mixing. Phys. Stat. Sol. **102**, 199 (1987)

45. Zhang, B., Tao, Z.: Prediction of the formation of binary metal-metal amorphous alloys by ion implantation. J. Mater. Sci. Lett. **7**, 681 (1988)